BBA - Molecular Basis of Disease 1868 (2022) 166384

Contents lists available at ScienceDirect

BBA - Molecular Basis of Disease

journal homepage: www.elsevier.com/locate/bbadis

Clusterin in Alzheimer's disease: An amyloidogenic inhibitor of amyloid formation?

Panagiotis M. Spatharas [a,1], Georgia I. Nasi [a], Paraskevi L. Tsiolaki [a,2], Marilena K. Theodoropoulou [a], Nikos C. Papandreou [a], Andreas Hoenger [b], Ioannis P. Trougakos [a], Vassiliki A. Iconomidou [a,*]

[a] Section of Cell Biology and Biophysics, Department of Biology, School of Sciences, National and Kapodistrian University of Athens, Panepistimiopolis, Athens 157 01, Greece

[b] University of Colorado at Boulder, Department of Molecular, Cellular and Developmental Biology, Boulder, CO 80309-0347, USA

ARTICLE INFO

Keywords:
Clusterin
Aggregation-prone regions
Amyloid
Amyloid-β
Amyloid inhibitors
Alzheimer's disease

ABSTRACT

Clusterin is a heterodimeric glycoprotein (α- and β-chain), which has been described as an extracellular molecular chaperone. In humans, clusterin is an amyloid-associated protein, co-localizing with fibrillar deposits in several amyloidoses, including Alzheimer's disease. To clarify its potential implication in amyloid formation, we located aggregation-prone regions within the sequence of clusterin α-chain, *via* computational methods. We had peptide-analogues, which correspond to each of these regions, chemically synthesized and experimentally demonstrated that all of them can form amyloid-like fibrils. We also provide evidence that the same peptide-analogues can inhibit amyloid-β fibril formation, potentially making them appropriate drug candidates for Alzheimer's disease. At the same time, our findings hint that the respective aggregation-prone clusterin regions may be implicated in the molecular mechanism in which clusterin inhibits amyloid formation. Furthermore, we suggest that molecular chaperones with amyloidogenic properties might have a role in the regulation of amyloid formation, essentially acting as functional amyloids.

1. Introduction

Since the 17th century, physicians had already started to describe clinical disorders that were later included in a broad group of diseases, nowadays known as amyloidoses [1]. Prime examples are Alzheimer's disease (AD), Parkinson's disease, type 2 diabetes, and amyloid light chain amyloidosis [2]. It is widely considered that these diseases are closely associated with the accumulation and close packing of normally soluble proteins, which end up creating highly ordered, insoluble aggregates. The so-called amyloid fibrils, are deposited extracellularly in organs or tissues, causing significant damage [2].

Molecular chaperones can inhibit amyloid formation in its early stages, thus preventing amyloid-related cytotoxicity [3]. Recent studies, though, have shown that molecular chaperones can have amyloidogenic properties [4–7], despite their seemingly contradicting physiological function. *In vitro* experiments performed by our team have hinted that clusterin could be such a protein [7]. Clusterin is a ubiquitous, conserved mammalian glycoprotein, whose main isoform is secreted and has been described as an extracellular molecular chaperone [8]. Human clusterin precursor is a 449 residue-long polypeptide chain, which, after having its signal peptide removed, is reduced to 427 residues, and goes through several post-translational modifications [8]. Mature clusterin is cleaved in two chains —α-chain, consisting of 222 residues, and β-chain, consisting of 205 residues— with five disulfide bonds forming between

Abbreviations: Aβ, Amyloid-β; AD, Alzheimer's Disease; ATP, Adenosine Triphosphate; ATR FT-IR, Attenuated Total Reflectance Fourier Transform Infrared; CLU, Clusterin; FAD, Familial Alzheimer's Disease; HFIP, 1,1,1,3,3,3-Hexafluoro-2-propanol; MP, Misfolded Proteins; NP, Native Proteins; RMSD, Root Mean Square Deviation; RMSF, Root Mean Square Fluctuation; sHSP, small Heat Shock Protein; TEM, Transmission Electron Microscopy; ThT, Thioflavin T.

* Corresponding author.

E-mail addresses: panspatharas@biol.uoa.gr (P.M. Spatharas), gnasi@biol.uoa.gr (G.I. Nasi), etsiolaki@biol.uoa.gr (P.L. Tsiolaki), mtheod@biol.uoa.gr (M.K. Theodoropoulou), npapand@biol.uoa.gr (N.C. Papandreou), Andreas.Hoenger@Colorado.edu (A. Hoenger), itrougakos@biol.uoa.gr (I.P. Trougakos), veconom@biol.uoa.gr (V.A. Iconomidou).

[1] Present Address: European Molecular Biology Laboratory, Hamburg Unit, Notkestrasse 85, 22,607 Hamburg, Germany.

[2] Present Address: Department of Biochemistry and Biophysics, University of California, San Francisco, California 94,143–2240, USA.

https://doi.org/10.1016/j.bbadis.2022.166384
Received 9 August 2021; Received in revised form 20 February 2022; Accepted 7 March 2022
Available online 13 March 2022

them [8]. Its apparent molecular mass is approximately 80 kDa, almost 30% of it being carbohydrates, added by glycosylation [8]. Clusterin's structure has yet to be experimentally determined, but is believed to contain three long molten globule-like regions and five amphipathic α-helices, which allow for hydrophobic interactions with its client-proteins [9].

Under normal circumstances, clusterin exists in solution as heterogeneous aggregates [10]. It has been suggested that, at mildly acidic pH [10], these aggregates disassociate and the disassociated chaperone-active subunits function in an ATP-independent manner [11]. They bind misfolded client-proteins and form a high molecular weight complex. The formation of the complex allows for stabilization of the misfolded proteins, which are consequently refolded by other molecular chaperones [9] (visualized in Fig. 1). Clusterin's ever-growing list of known clients includes a variety of proteins, such as cellular receptors, apolipoproteins, complement system proteins, immunoglobulins, and amyloid-forming proteins [12].

Having such a broad range of clients, it is only logical that clusterin contributes to many physiological and pathological processes [13]. AD is one of the most notable pathologies in which clusterin is involved [12]. Consistent with its chaperone function, clusterin keeps the amyloid-β (Aβ) peptide soluble while transporting it in biological fluids, modulates its permeation through the blood-brain barrier, and contributes to its clearance, effectively inhibiting amyloid formation [14]. In direct contradiction to that, it has been reported that clusterin contributes to the early stages of AD pathogenesis [15,16]. To this day, clusterin's role in AD is yet to be fully understood. Despite the mystery surrounding clusterin's implication in AD, it is a known fact that it co-localizes with Aβ fibrillar deposits [12]. This is also true for other amyloidoses, in which clusterin is an amyloid-associated protein [17].

It can be assumed that clusterin is found in the amyloid deposits because it is drifted along by its client-proteins. In this study, we examined a different scenario, one that doesn't rule out the possibility of clusterin being amyloidogenic itself. We used AMYLPRED, a consensus algorithm that utilizes 5 individual methods for the prediction of amyloid propensity [18], in order to identify aggregation-prone regions in clusterin α-chain. Using a protein's amino acid sequence as input, AMYLPRED can locate parts of the sequence that have a high propensity to be implicated in protein misfolding and amyloid formation. A protein region is predicted as aggregation-prone, if at least 2 out of 5 individual methods agree (see Section 5.1). We had peptide-analogues of each predicted region chemically synthesized and experimentally demonstrated that all of them can form amyloid-like fibrils *in vitro*. The same peptide-analogues, despite being amyloidogenic, can inhibit Aβ fibril formation. Based on our findings, we proposed a putative mechanism in which clusterin prevents amyloid formation. The suggested mechanism could also explain the contradictory reports that hint at clusterin's implication in the acceleration of the appearance of AD symptoms. At the same time, we hope that the basis of clusterin's amyloid inhibiting activity could give insight into the implementation of peptide-based amyloidogenesis inhibitors in the treatment of amyloidoses.

2. Results

2.1. All wild-type clusterin α-chain peptide-analogues form amyloid-like fibrils in vitro

According to the prediction of AMYLPRED, clusterin α-chain has five aggregation-prone regions. The peptide-analogues that correspond to those regions are NFHAMFQ, AMDIHF, ILSVD, YYLRVTT, and EVVVKLF, as depicted in Fig. 2. NFHAMFQ has previously been studied by our lab and proved to exhibit amyloidogenic properties *in vitro* [7]. Our current findings reveal that AMDIHF, ILSVD, YYLRVTT, and EVVVKLF can also be characterized as amyloidogenic *in vitro*, making a total of five experimentally verified aggregation-prone regions in clusterin α-chain. Characterization was based on the tinctorial criteria, which are commonly used for the identification of amyloid fibrils (transmission electron microscopy, X-ray diffraction from protein fibers, ATR FT-IR spectroscopy, and Congo Red birefringence assay) [19].

Transmission electron micrographs show that AMDIHF, ILSVD, YYLRVTT, and EVVVKLF self-assemble into amyloid-like fibrils (Fig. 3 A-D, respectively). AMDIHF fibrils exhibit considerable polymorphism, forming both supercoils and tapes (Fig. S1 A-C), while EVVVKLF fibrils form large twisting ribbons, with a 162 nm pitch (Fig. S1D). ILSVD forms amyloid-like fibrils that are packed more densely in comparison to the other peptides (Fig. 3), indicating that it could be the most aggregation-prone region in clusterin α-chain.

Oriented fibers formed by each peptide solution, produce X-ray

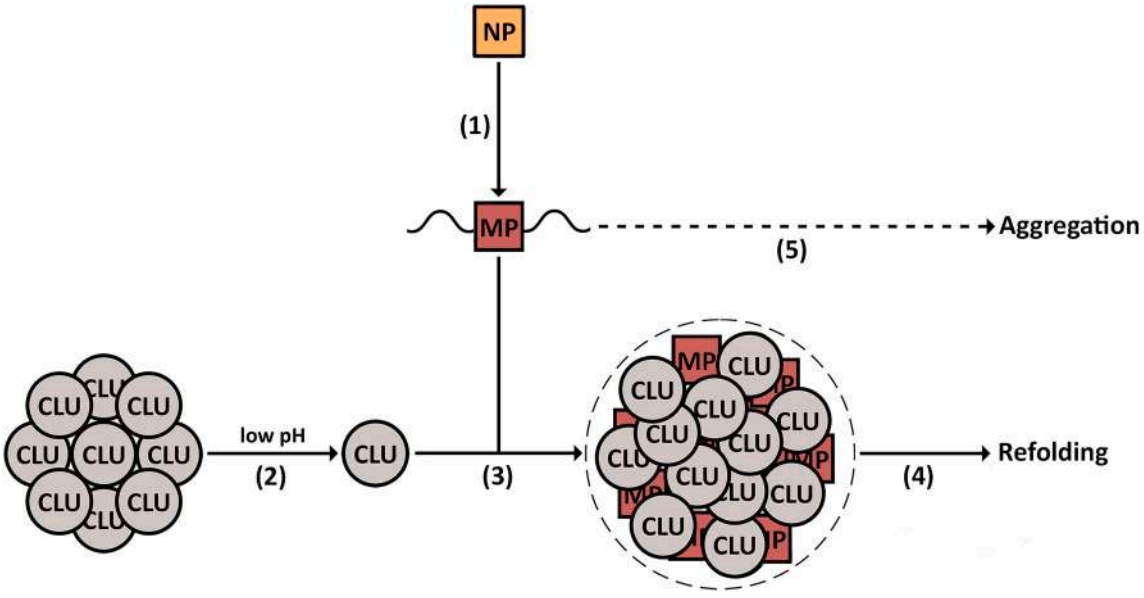

Fig. 1. Representation of clusterin's molecular chaperone activity. (1) Under stress (low pH), native proteins (NP) may partially unfold and become misfolded. (2) At slightly acidic pH, clusterin's (CLU) oligomers start disassociating and the chaperone-active clusterin subunits get released. (3) The free clusterin subunits bind the misfolded proteins (MP) and form a complex, effectively stabilizing them, (4) while other molecular chaperones refold them to their native state. (5) If this mechanism proves ineffective, the misfolded proteins may form aggregates.

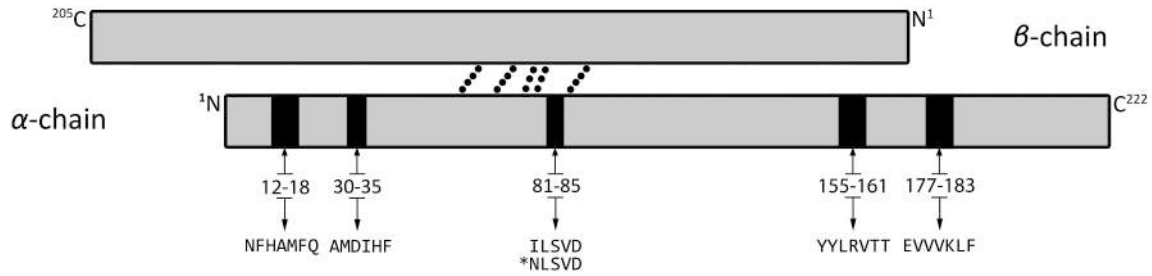

Fig. 2. A simple representation of clusterin's two chains. Each chain is colored grey, with a black outline, and its sequence is numbered as found in the mature protein. The α-chain consists of 222 amino acid residues. The β-chain is slightly shorter, consisting of 205 amino acid residues. The two chains are joined by five disulfide bonds, depicted as black dots. The aggregation-prone regions of the α-chain are depicted as black rectangles on clusterin's sequence.

diffraction patterns, indicative of the presence of the "cross-β" structure. Most reflections are ring-like, most likely because the fibrils are not perfectly aligned in a parallel manner [20]. The exact measurements for each of the four diffraction patterns can be seen in Fig. 3 (E-H). It is worth pointing out that the EVVVKLF diffraction pattern has two equatorial reflections, one at 8.12 and one at 12.12 Å. Upon closer examination of the twisting ribbons, formed by EVVVKLF (Fig. S1D), the maximum width is observed in the middle of the pitch, and measures approximately 53 nm, while the minimum width is observed at the site of the twist, and measures approximately 35 nm. The quotient of the two equatorial reflections (8.12/12.12 ≈ 0.67) is roughly equal to the quotient of the minimum and maximum ribbon width (35/53 ≈ 0.66). The equatorial reflections are indicative of the distance between packed β-sheets. Thus, EVVVKLF fibrillar structures are probably formed by β-sheets that are more tightly packed at the twist, in comparison to the middle of the ribbon. The periodicity of the tightening and untightening of the β-sheets is revealed by a combination of X-ray and TEM data.

The dominance of the β-sheet secondary structure is supported by ATR FT-IR spectroscopy data, since the spectra of all four peptide-analogues reveal bands that can be assigned to β-sheets [21] (Table 1 and Fig. 3 M-O).

Every peptide binds Congo Red, as seen under bright field illumination in a polarizing stereomicroscope (Fig. 3 I-L, upper). When the polars are crossed, the peptides exhibit the apple-green birefringence (Fig. 3 I-L, lower) that amyloids typically exhibit.

2.2. NLSVD, a mutant counterpart of ILSVD, does not exhibit amyloidogenic properties

Recent studies have identified a novel pathological mutation on clusterin's gene, in AD patients. In particular, p.I360N changes the aggregation-prone region ^{81}ILSVD^{85} to ^{81}NLSVD^{85} [22]. The resulting sequence is not predicted by AMYLPRED, hinting that it is not aggregation-prone. To experimentally confirm that the mutated region is not aggregation-prone, we had NLSVD chemically synthesized. Indeed, transmission electron microscopy (TEM) shows that NLSVD does not self-assemble into amyloid fibrils (Fig. S2A). Also, NLSVD does not form oriented fibers, suitable for X-ray diffraction, hinting that there are no fibrils in its solution. Finally, when stained with Congo Red and stereoscopically observed between crossed polars, it does not exhibit apple-green birefringence (Fig. S2B).

2.3. Clusterin α-chain peptide-analogues inhibit $A\beta_{42}$ amyloid formation in vitro

Full-length clusterin is known to inhibit Aβ fibril formation *in vitro* [23]. We aimed to pinpoint segments of its sequence that could act as catalysts of said inhibition. Each clusterin peptide-analogue was co-incubated with equimolar amounts of $A\beta_{42}$ and the aggregation kinetics were evaluated with Thioflavin T (ThT) fluorescence measurements over time, as well as TEM.

ThT fluorescent measurements reveal that individual $A\beta_{42}$ starts forming fibrils almost immediately and reaches maximal fluorescence signal after approximately 7 h. When co-incubated with clusterin peptide-analogues ($A\beta_{42}$ + NFHAMFQ, $A\beta_{42}$ + AMDIHF, $A\beta_{42}$ + ILSVD, $A\beta_{42}$ + YYLRVTT, and $A\beta_{42}$ + EVVVKLF), $A\beta_{42}$ exhibits decreased emission. ILSVD and especially EVVVKLF seem to be the most potent inhibitors (Fig. 4J and P, respectively). As previously shown, individual ILSVD is incredibly amyloidogenic, as is $A\beta_{42}$. The fact that interaction between the two leads to decreased fibril formation, hints those peptides with high amyloidogenic potential, could negate each other's fibril-forming properties. EVVVKLF bears some sequence similarity with ^{16}KLVFFA^{21}, a key amyloid-forming segment of $A\beta_{42}$ [24]. Considering that peptide-analogues derived from ^{16}KLVFFA^{21} have been suggested as potential therapeutic agents for the treatment of AD [25], it is not surprising that EVVVKLF has the highest inhibiting effect among the five peptides. NFHAMFQ and AMDIHF also seem to inhibit $A\beta_{42}$ fibril formation (Fig. 4F and H, respectively), but their potential as inhibitors is less significant than that of ILSVD and EVVVKLF. YYLRVTT effectively delays fibril formation, but after approximately 20 h, fluorescence signal begins to rise (Fig. 4N). After 40 h, $A\beta_{42}$ + YYLRVTT reaches fluorescence intensity levels which are comparable to those of individual $A\beta_{42}$.

It is worth mentioning that none of clusterin's peptide-analogues show enhanced fluorescence when incubated individually in the concentration that $A\beta_{42}$ was incubated (10 μM) (Fig. S4). In higher concentrations (100 μM), all peptides form fibrils, as previously showcased (Fig. 3). This fact hints that in lower concentrations, these peptides might be soluble, making them appealing as peptide-drug candidates.

TEM confirms that all five peptide-analogues inhibit or delay $A\beta_{42}$ fibril formation, after 7 days of incubation. When individually incubated, $A\beta_{42}$ forms straight and unbranched fibrils with indefinite length and a diameter of approximately 80 Å (Fig. 4 B—D). A small number of fibrils is observed after 1 day of incubation (Fig. 4B). The population of fibrils increases significantly after 3 days (Fig. 4C) and reaches its maximum after 7 days (Fig. 4D). As expected, ILSVD and EVVVKLF prove to be the most potent inhibitors (Fig. 4I and O, respectively). The entire grids were thoroughly examined, and no fibrils were observed. NFHAMFQ and AMDIHF also inhibit $A\beta_{42}$ fibril formation, as fibrils were not observed anywhere on the grid (Fig. 4E and G, respectively). However, both seem to induce the formation of amorphous aggregates. YYLRVTT seems to delay, but not inhibit fibril formation. In contrast to the other peptides, fibrils can be observed (Fig. 4M). The number of fibrils is similar to that of individual $A\beta_{42}$, after 1 day of incubation. Much like NFHAMFQ and AMDIHF, YYLRVTT also seems to induce the formation of amorphous aggregates.

On the contrary, ThT kinetics and TEM show that NLSVD, the mutant counterpart of ILSVD, does not inhibit $A\beta_{42}$ amyloid formation *in vitro*. $A\beta_{42}$ and $A\beta_{42}$ + NLSVD fluorescence curves mostly overlap, while $A\beta_{42}$ + NLSVD show a slightly enhanced fluorescence peak (Fig. 4K). Transmission electron micrographs reveal that $A\beta_{42}$ fibril morphology is different from that of $A\beta_{42}$ + NLSVD. Aβ + NLSVD fibrils, after 7 days of incubation, are more densely packed and slightly wider than those of

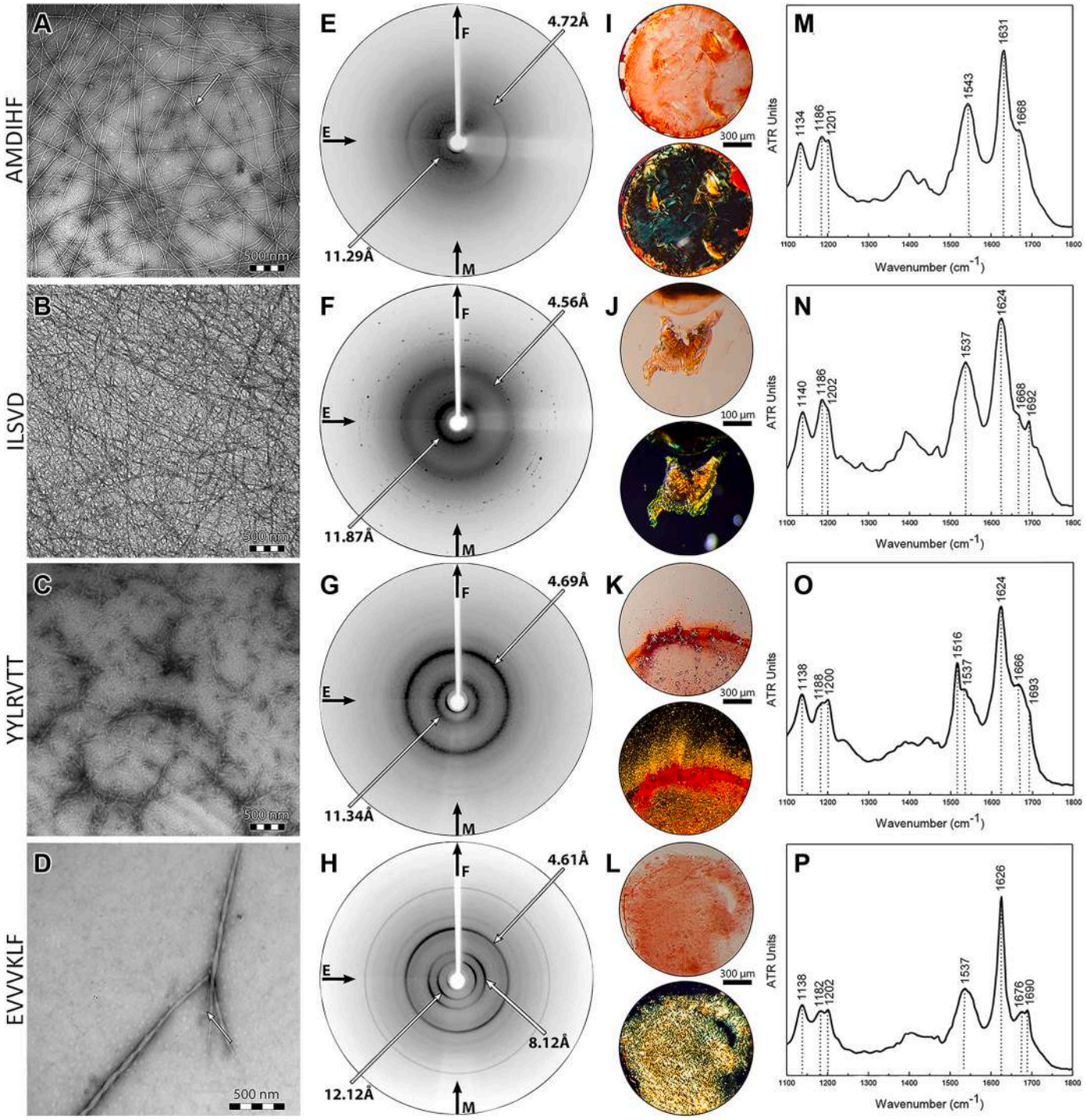

Fig. 3. All the peptide-analogues fulfill the experimental criteria. (A-D) Transmission electron micrographs of amyloid-like fibrils derived from 500 μm solutions of peptides AMDIHF, ILSVD, YYLRVTT, and EVVVKLF, respectively. White arrows mark single fibrils with the diameter of typical amyloid fibrils. (E-H) X-ray diffraction patterns of oriented fibers, derived from 1 mM solutions of the four peptides, respectively. Reflections marked with arrows are indicative of the "cross-β" structure, which amyloids typically have. (I-L) Photomicrographs of gels, derived from 500 μM solutions of the four peptides, respectively. Congo red is bound, as seen under bright field illumination (upper). The apple-green birefringence that amyloids typically exhibit is observed under crossed polars (lower). (M-P) ATR FT-IR spectra (1100–1800 cm^{-1}) produced from thin hydrated films created by 500 μM solutions of the four peptides, respectively. Fibrils derived from each peptide have a β-sheet secondary structure, as hinted by the presence of strong amide I and II bands. All experiments were performed three times. (For interpretation of the references to colour in this figure legend, the reader is referred to the web version of this article.)

individual Aβ_{42}, after the same incubation period (Fig. 4L and Fig. S2C, white arrow). Furthermore, Aβ_{42} + NLSVD fibrils tend to interact laterally and form loosely bound tapes (Fig. S2C, blue arrows).

To pinpoint potential cooperative/interferential activity among the 5 peptide-analogues, we co-incubated all of them with Aβ_{42} in the same reaction solution. ThT kinetics show that Aβ_{42} still exhibits decreased fluorescence emission (Fig. S4C), but the results are not as pronounced as with each individual peptide. TEM, in accordance with ThT kinetics, reveals that Aβ_{42} fibril formation is inhibited (Fig. S4A). In summary, although the peptides still act as inhibitors when in the same solution,

Table 1
Bands observed in the ATR FT-IR spectra obtained from thin hydrated films produced by AMDIHF, EVVVKLF, YYLRVTT, and ILSVD solutions, respectively, and their tentative assignments.

AMDIHF bands	ILSVD bands	YYLRVTT bands	EVVVKLF bands	Band assignments
1134	1140	1138	1138	TFA
1186	1186	1188	1182	TFA
1201	1202	1200	1202	TFA
–	–	1516	–	Tyrosine
1543	1537	1537	1537	β-sheet
1631	1624	1624	1626	β-sheet
1668	1668	1666	1676	TFA
–	1692	1693	1690	Antiparallel β-sheet

their inhibitory effect is reduced. Interestingly, the inclusion of NLSVD in the reaction solution does not drastically change the outcome (Fig. S4D), although some short fibril segments can be observed in transmission electron micrographs (Fig. S4B).

2.4. Computational insight into the inhibition of $A\beta_{42}$ fibril formation by EVVVKLF

To shed light on the interaction between Aβ_{42} and EVVVKLF, the most potent of the five peptide-inhibitors, molecular dynamics simulations were performed, using an NMR structure of pentameric Aβ_{42} (PDB ID: 2BEG) [26]. A structure for EVVVKLF was generated through the "Builder" tool in PyMOL [27]. Molecular docking was performed through the automated protein docking server ClusPro [28–31]. The generated clusters were evaluated with the balanced scoring scheme. Following energy minimization, the interaction between Aβ_{42} key amyloid-forming segment ^{17}LVFFA^{21} (Fig. 5A, dark grey) and EVVVKLF (Fig. 5A, light grey) was ascertained (Fig. 5A, left).

Aβ_{42} + EVVVKLF complex structural stability was monitored through per-residue root mean square fluctuation (RMSF) calculation, as well as time-dependent root mean square deviation (RMSD) measurements (Fig. 5B and C, respectively). After 600 ns of molecular dynamics simulations, a complex dissociation has occurred, significantly changing the conformation of the pentamer, in comparison to its original state (Fig. 5A). The C-termini of all five chains are characterized by large fluctuations (0.4–0.8 nm), with chains-A and —B exhibiting the highest mobility. In contrast, the N-termini of the aforementioned chains exhibit the lowest mobility among all chains, while the chain-E N-terminus is characterized by fluctuations of over 0.8 nm. Secondary structure analysis was performed using the dictionary of secondary structure of proteins (DSSP) algorithm [32,33] and reveals that β-sheet content gradually decreases (Fig. 5D). Intermolecular hydrogen bonds are formed, even before the simulation has begun, and reach a maximum number of 12 (Fig. 5E). Upon examination of the last frame of the simulation (Fig. 5A, right), EVVVKLF has partly adopted a β-strand conformation. Using UCSF Chimera and the "FindHBond" tool [34], we show that EVVVKLF forms three possible hydrogen bonds with the chain-A ^{16}LVFFA^{21} region, becoming a part of an intermolecular β-sheet. EVVVKLF also forms hydrogen bonds with the C-terminus of the A-chain. By forming hydrogen bonds with both regions, it essentially "stitches" the N-terminal ^{17}LVFFA^{21} to the C-terminus. The fact that RMSF values are low for the N-terminus and high for the C-terminus hints that the latter moves towards the former. In this way, fibril elongation from chain-A could be blocked. The addition of more than one peptide-inhibitors could promote interactions with chain-E, effectively blocking both elongation epitopes of the pentamer.

2.5. AlphaFold-Multimer gives insight into the relative positions of aggregation-prone regions in full-length clusterin

AlphaFold-Multimer [35–39] reveals that clusterin has a mostly α-helical structure with many flexible regions (Fig. 6A). Prediction accuracy data are included in Fig. S5. Secondary structure data was extracted using STRIDE [40] (Fig. 6B). Based on this model, all 5 aggregation-prone regions are located near flexible regions (turns or coils). ^{12}NFHAMFQ^{18} is on the right of the α-chain N-terminal coil/turn, which is thought to be natively disordered [9]. ^{30}AMDIHF^{35} and ^{81}ILSVD^{85} are on the left of turn/coil regions, while ^{155}YYLRVTT^{161} and ^{177}EVVVKLF^{183} are surrounded by coils/turns. The proximity of all five aggregation-prone regions to coils/turns may hint that, due to the flexibility of the latter, the former could act semi-independently of the protein.

Another interesting observation is that ^{12}NFHAMFQ^{18} and ^{30}AMDIHF^{35} seem to be a part of an α-helix, which has been shown to be amphipathic [9]. Amphipathic α-helices are believed to be implicated in the interaction between clusterin and its client proteins [9], suggesting that both regions may have a role in the stabilization of misfolded proteins.

It also worth noting that, although all 5 aggregation-prone regions are mostly hydrophobic, they seem to be located on the surface of clusterin (Fig. 6A, lower). Hydrophobic regions are usually buried in the protein core, avoiding contact with the surrounding aqueous solution. The exposure of the aggregation-prone regions to the protein surface points, once again, the possibility of a functional role.

However, AlphaFold does not take into account the multiple post-translational modifications, which clusterin undergoes. Modification sites have been marked on the model (Fig. 6, orange for glycosylation, blue for phosphorylation), to give a sense of relative positioning between them and the aggregation-prone regions. Interestingly, most post-translational modification sites seem to not be in close proximity to the aggregation-prone-regions, both in clusterin's structure (Fig. 6A) and sequence (Fig. 6B). A phosphorylation site (α-chain serine 169) is located between ^{155}YYLRVTT^{161} and ^{177}EVVVKLF^{183}, while a glycosylation site (α-chain asparagine 147) is relatively near ^{155}YYLRVTT^{161} in sequence and ^{30}AMDIHF^{35} in structure. The effects of these modifications on clusterin's structure remain largelyl unknown.

3. Discussion

3.1. Full-length clusterin might have amyloidogenic properties, which could be implicated in its function

Recent studies have shown that short aggregation-prone segments, known as amyloidogenic determinants, can lead to amyloid formation, even when they are inserted in non-amyloidogenic proteins, *via* protein engineering [41]. The fact that clusterin has five such segments in its α-chain, provides potent indication that the α-chain and consequently the full-length protein, may intrinsically exhibit amyloidogenicity. Clusterin β-chain has another 7 predicted aggregation-prone regions [7], which were not experimentally tested in the current study, and potentially add to full-clusterin's amyloidogenic propensity.

In addition to their amyloidogenic properties, the 5 experimentally tested peptides inhibit amyloid fibril formation by Aβ_{42} *in vitro*. This finding was used as proof of concept to show that amyloidogenic peptides can have anti-amyloidogenic properties. The same could also be true for the 7 remaining predicted regions of clusterin β-chain, but this remains to be determined. Additionally, there might be more regions that exhibit similar properties but are not predicted by AMYLPRED, due to the inaccuracy of current predictive methods. For example, ^{113}LVGRQLEEFL^{122} is a region of clusterin β-chain, whose peptide-analogue has been reported to improve cognitive function and reduce Aβ plaques in an AD transgenic model, after injection [42]. Another explanation for its anti-fibrillogenic activity would be the 3 charged

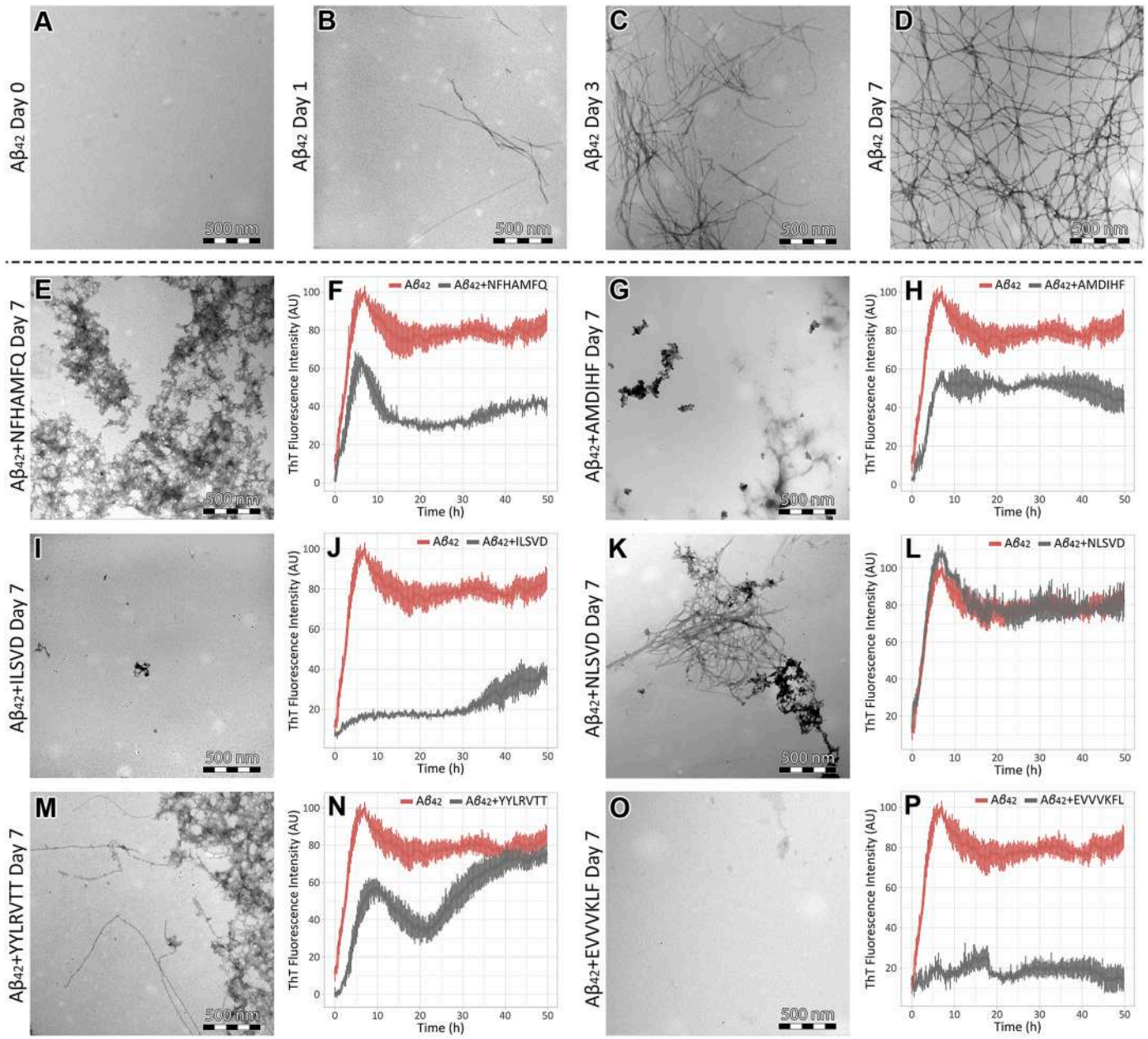

Fig. 4. Clusterin peptide-analogues inhibit or delay Aβ_{42} fibril formation. (A-D) Transmission electron micrographs of Aβ_{42}, incubated for 0, 1, 3, and 7 days, respectively. Amyloid fibrils are observed from day 1 to day 7. The number of fibrils raises as incubation time increases. (E, F) Transmission electron micrograph and ThT fluorescence emission spectrum of Aβ_{42} co-incubated with NFHAMFQ for 7 days and over a period of 50 h, respectively. (G, H) Transmission electron micrograph and ThT fluorescence emission spectrum of Aβ_{42} co-incubated with AMDIHF for 7 days and over a period of 50 h, respectively. (I, J) Transmission electron micrograph and ThT fluorescence emission spectrum of Aβ_{42} co-incubated with ILSVD for 7 days and over a period of 50 h, respectively. (K, L) Transmission electron micrograph and ThT fluorescence emission spectrum of Aβ_{42} co-incubated with the mutant peptide, NLSVD, for 7 days and over a period of 50 h, respectively. (M, N) Transmission electron micrograph and ThT fluorescence emission spectrum of Aβ_{42} co-incubated with YYLRVTT for 7 days and over a period of 50 h, respectively. (O, P) Transmission electron micrograph and ThT fluorescence emission spectrum of Aβ_{42} co-incubated with EVVVKLF for 7 days and over a period of 50 h, respectively. Error bars in ThT fluorescence emission spectra represent standard deviation among triplicates. TEM experiments contained 100 μM Aβ_{42} and 100 μM clusterin peptide-analogues, while ThT experiments contained 10 μM and 10 μM, respectively. All experiments were performed three times.

resides that it contains, which make it a potential β-strand breaker.

The arguments of the 2 previous paragraphs have fascinating implications if combined, especially considering clusterin's role as a molecular chaperone. Of course, definitive conclusions about its function are subject to validation, using the full-length protein, which was not the focus of the current study.

3.2. Molecular chaperones and their involvement in amyloid formation and inhibition

One of the fundamental functions of molecular chaperones is considered to be the prevention of protein aggregation and consequently, amyloid fibril formation [3]. Based on that notion, it has been suggested that molecular chaperones could be used as anti-amyloid drugs [43]. In direct contradiction to that, clusterin regions have the potential to form amyloid-like fibrils. In fact, there have been reports of

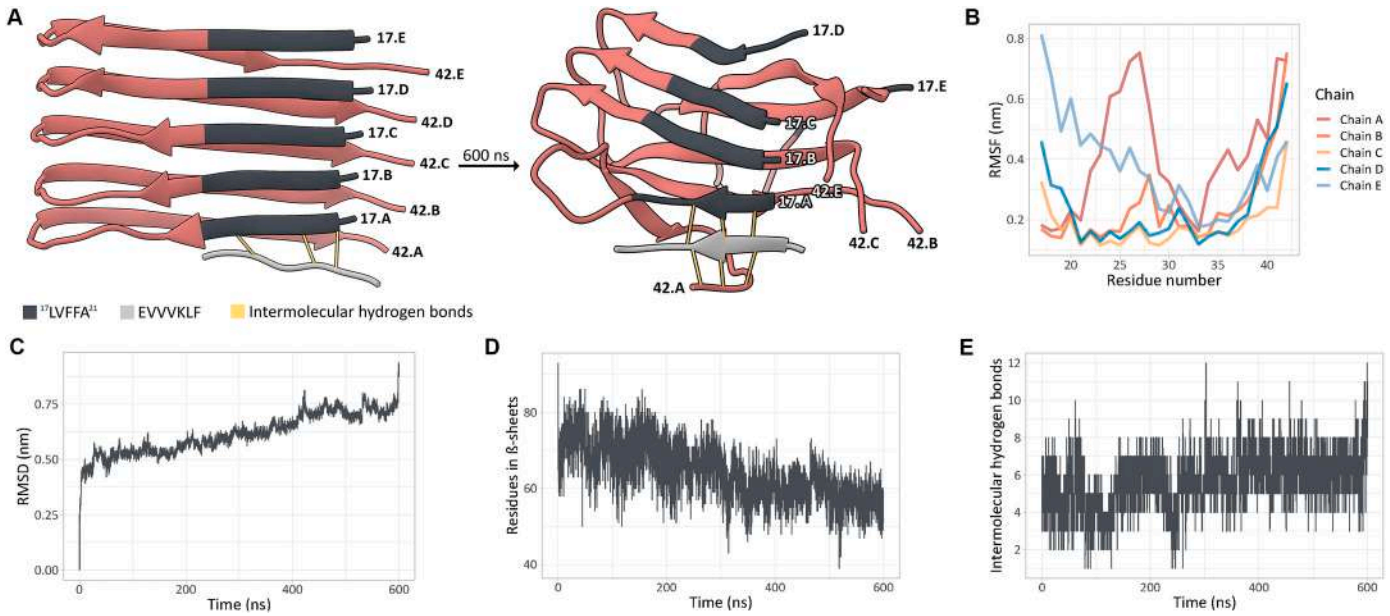

Fig. 5. Results of molecular dynamics simulations for Aβ_{42} + EVVVKLF. (A) First (0 ns, left) and last (600 ns, right) frames of the molecular dynamics simulation. The positions of the N- and C-terminals of each Aβ_{42} chain are marked on each frame (17.A-17.E and 42.A-42.E, respectively). EVVVKLF (light grey) forms hydrogen bonds (yellow lines) with the chain-A ^{17}LVFFA^{21} (dark grey), right after molecular docking and energy minimization. More bonds are formed by the end of the simulation. (B) RMSF per residue plot, after 600 ns of molecular dynamics simulations. (C) RMSD over time plot. (D) The total number of residues in β-sheets, according to DSSP, over time. (E) Number of intermolecular hydrogens bonds, between Aβ_{42} and EVVVKLF, over time. (For interpretation of the references to colour in this figure legend, the reader is referred to the web version of this article.)

other proteins that function as molecular chaperones and exhibit amyloidogenicity *in vitro* [5,6] or *in vivo* [4]. Despite lacking any sequence similarity, this group of proteins shares a significant number of similar features, besides having the potential to form amyloid-like fibrils.

A prominent example is α-crystallin, a small heat shock protein (sHSP), which is highly expressed in the eye lens. Full-length α-crystallin has been found to form amyloid-like fibrils *in vitro* [5] and is believed to be implicated in the formation of cataract [44]. As most sHSPs, α-crystallin exhibits remarkable structural plasticity, which is intertwined with its chaperone activity [45]. Interestingly, α-crystallin's chaperone activity is exhibited in a very similar manner to that of clusterin [46]. sHSPs exist in solution as oligomeric structures, ranging from 9 to 50 subunits. Those structures disassociate under stress and release functional subunits [47]. α-crystallin in particular, possesses a dynamic oligomeric structure, which, under increasing temperature, allows the exchange of subunits within proximate oligomers. The so-called "traveling subunits" are believed to play a fundamental role in α-crystallin's chaperone activity, by exposing hydrophobic surfaces and consequently, allowing hydrophobic interactions with misfolded proteins, including Aβ [48–50]. Even though this is the physiological mechanism in which α-crystallin functions, it is reminiscent of how amyloidogenic proteins behave on their way to self-assembly and formation of amyloid fibrils [51]. This might explain the reports of α-crystallin forming amyloid-like fibrils *in vitro* [5].

Another relevant example is that of the caseins, a group of proteins that comprise the largest part of the total protein content in milk [52] and are usually found in aggregates, known as casein micelles. The micelles are primarily composed of four major proteins, namely α_{s1}-, α_{s2}-, β- and κ-casein [53]. All four of them have been classified as intrinsically disordered proteins, because of the considerable structural flexibility that they exhibit [54]. In consistence with clusterin and α-crystallin, the major casein proteins are believed to function as molecular chaperones [55], while κ-casein forms amyloid fibrils *in vitro* [6] and α_{s2}-casein forms amyloid fibrils *in vivo*, in corpora amylacea, in the bovine mammary gland [2,4]. Yet, in physiological conditions, α_{s1}-casein interacts with α_{s2}-casein, forming α_s-casein, effectively halting the formation of amyloid fibrils [56]. Similarly, α_s-casein and β-casein inhibit κ-casein amyloid formation, by shielding monomeric κ-casein hydrophobic surfaces with similar regions of their respective sequences [57].

In summary, clusterin, α-crystallin, and the casein proteins share common features:

(1) They function as molecular chaperones, by exposing hydrophobic regions, interacting with and stabilizing misfolded proteins on their way to aggregation.
(2) They show structural plasticity, either having molten globule-like or intrinsically disordered regions on their sequence.
(3) They are found in solution as heterogeneous aggregates, oligomers, or micelles, which dissociate under conditions of stress.
(4) They all interact with one, or more amyloidogenic proteins.
(5) Parts of their sequence, or the full-length proteins, are known to form amyloid-like fibrils *in vitro* or *in vivo*.

These similarities may underlie a common mechanism in which the cell prevents toxic amyloid formation under different conditions of stress, by utilizing the intrinsic amyloidogenicity of specific molecular chaperones. For clusterin, amyloidogenesis inhibition could be activated under pH-induced stress and achieved through the interaction of its aggregation-prone regions with amyloidogenic proteins, on their way to aggregation. Likewise, α-crystallin could act under temperature-induced stress and the casein proteins may present a more specific system of amyloid inhibition, present primarily at the mammary gland.

3.3. *A putative mechanism for clusterin-mediated inhibition of Aβ amyloidogenesis*

Clusterin α-chain peptide-analogues can inhibit Aβ amyloidogenesis *in vitro*. Based on the AlphaFold model, clusterin seems to have flexible regions in proximity to the exposed α-chain aggregation-prone regions. The structural flexibility that the former regions introduce, may enable the latter to act semi-independently of the protein. Having established

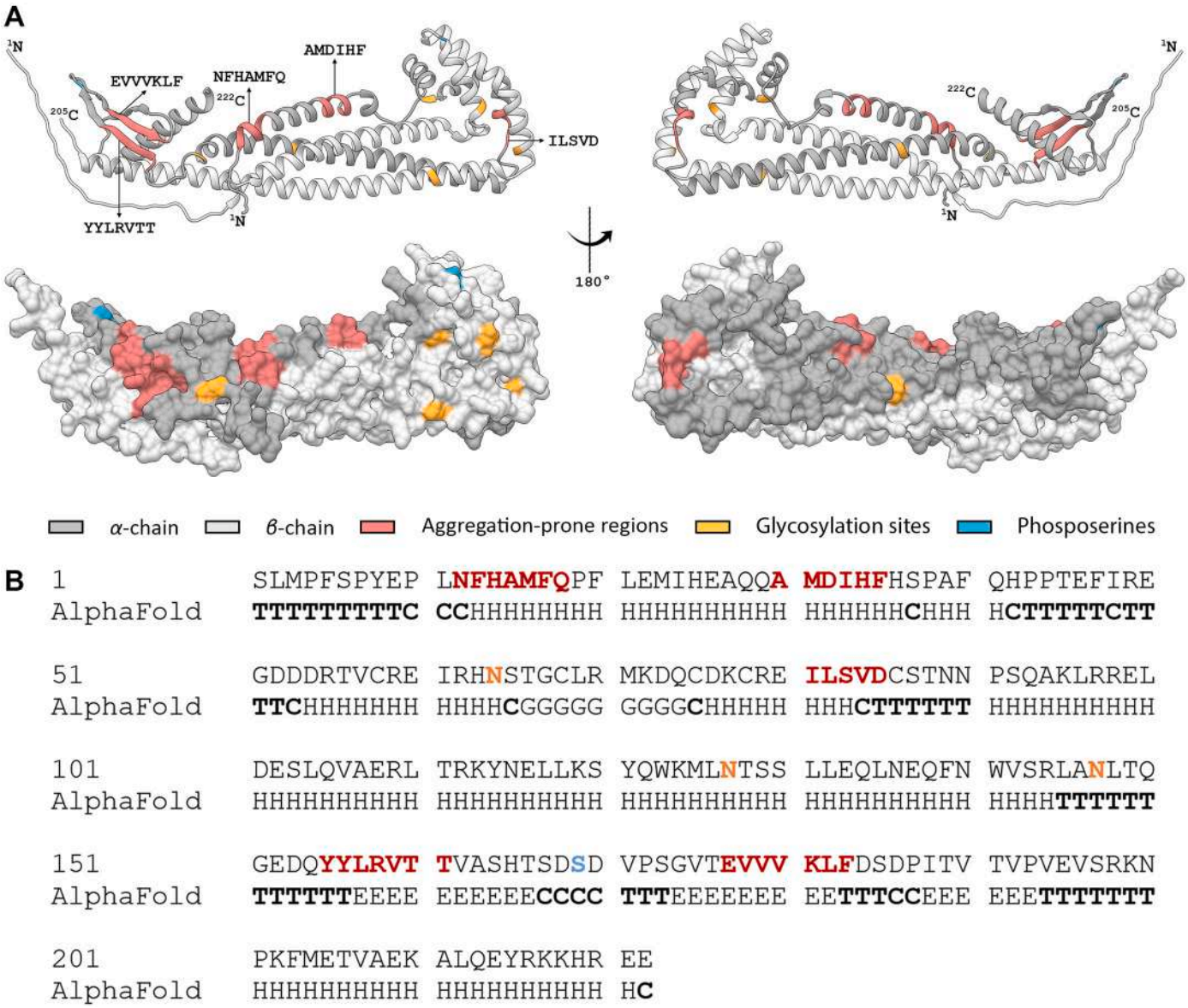

Fig. 6. Clusterin AlhpaFold-Multimer model. (A) Ribbon and surface representation of clusterin's structural model. The α-chain is colored dark grey, while the β-chain light grey. Aggregation-prone regions are colored red, glycosylation sites are colored orange, and phosphoserines are colored blue. (B) Secondary structure data for clusterin's α-chain sequence, extracted from the AlhpaFold structural model, using STRIDE. The coloring of the features of the sequence remains the same as before. Regarding the secondary structure, H is α-helix, E is β-strand, G is 3_{10}-helix, T is turn, and C is coil. Coils and turns (C and T) are depicted with bold letters. (For interpretation of the references to colour in this figure legend, the reader is referred to the web version of this article.)

that, we opted to propose a mechanism in which clusterin could use its aggregation-prone regions to exert its molecular chaperone activity on Aβ.

It is believed that Aβ amyloidogenesis is promoted by acidic pH [58]. As previously mentioned, mildly acidic pH also allows the disassociation of clusterin's heterogeneous aggregates, releasing chaperone-active subunits [10]. In its disassociated form, clusterin is assumed to hydrophobically interact with its client-proteins through amphipathic α-helices, which are surrounded by molten globule-like regions [9]. ^{12}NFHAMFQ^{18}, one of clusterin's aggregation-prone regions, is located on a putative amphipathic α-helix. However, we have already proved that NFHAMFQ also has the propensity to form β-strands [7], hinting that the broader region has the intrinsic conformational properties of a chameleon sequence. When in proximity with an Aβ fibril, the α-helical ^{12}NFHAMFQ^{18} could unfold and then refold into a β-strand, allowing interaction with Aβ's β-stranded regions and temporarily halting fibril growth. This process could trigger the exposition of clusterin's other aggregation-prone regions and allow it to attach itself at the edge of the Aβ fibril, *via* β-strand hydrogen bonding. In this manner, it would not allow Aβ monomers to elongate the fibril, effectively blocking further polymerization. At the same time, free clusterin subunits could bind to Aβ monomers, forming complexes and stabilizing their structure, until it passes the baton to other molecular chaperones, once again, halting fiber growth and minimizing the possibility of toxic secondary nucleation [59]. The suggested mechanism is visualized in Fig. 7.

The putative mechanism that was just described, is also supported by the identification of a pathological mutation on clusterin's gene, in AD patients. As previously mentioned, p.I360N changes the aggregation-prone region ^{81}ILSVD^{85} to ^{81}NLSVD^{85} [22]. Considering that out of the peptides we examined, ILSVD is hinted to be one of the better Aβ fibril formation inhibitors, this mutation could lead to a malfunction in the clusterin-mediated amyloidogenesis inhibition system. Thus, the pathogenicity of the phenotype could be explained by clusterin's inability to inhibit amyloid formation, due to the absence of its most

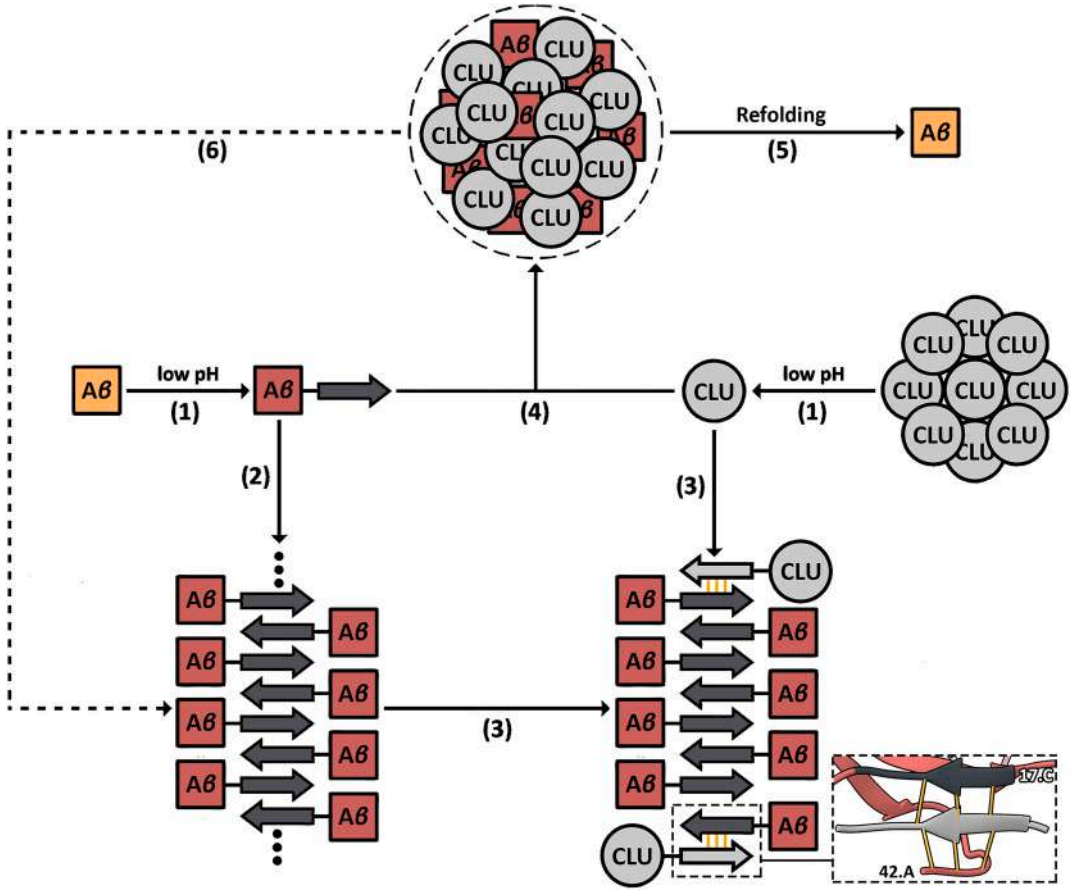

Fig. 7. Putative mechanism of clusterin-mediated inhibition of Aβ amyloidogenesis. (1) Under acidic pH-induced stress, Aβ may partially unfold, exposing hydrophobic regions with the propensity to form β-strands. At the same time, the acidic pH triggers the disassociation of clusterin's heterogeneous aggregates. (2) Misfolded Aβ begin to form amyloid fibrils, but (3) the disassociated clusterin subunits (CLU) halt fibril growth, utilizing their aggregation-prone regions, which tend to form β-strands as well. The outlined picture is derived from the last frame of the molecular dynamics simulation of $A\beta_{42}$ + EVVVKLF. (4) Clusterin binds misfolded Aβ monomers, forming complexes and stabilizes their structure, until (5) they are refolded by other molecular chaperones. (6) In case misfolded Aβ species are produced faster than clusterin can stabilize their structure, it essentially brings them into proximity with remote monomers, accelerating amyloid formation.

aggregation-prone region, that being ^{81}ILSVD^{85}, which would normally inhibit Aβ fibril formation.

The aforementioned mechanism can explain why clusterin is found co-localized with Aβ fibrillar deposits [12] and is consistent with reports of clusterin decelerating Aβ fibril formation [59,60]. However, clusterin's occasional contribution to the appearance of AD symptoms [15,16] needs further elucidation. It is logical to assume that, when Aβ misfolded monomers are produced faster than what clusterin's existing population can process, the resulting complexes would fail to stabilize Aβ's structure, essentially bringing remote misfolded monomers into proximity. This could accelerate amyloid fibril formation (Fig. 7 – 6), while clusterin would end up co-localized with the fibrillar deposits. This hypothesis is supported by the findings of Yerbury et al., which show that clusterin's enhancing effect on amyloid formation is caused by a low clusterin:substrate ratio [23]. A relevant example could be found in patients with familial Alzheimer's disease (FAD), where Aβ is produced much faster than usual [61]. In fact, most pre-clinical studies on AD use FAD animals as models, because it is a guaranteed method of acquiring early-onset AD test subjects [62]. This could also be the case for Oh *et. al*, who showed that clusterin-null 5XFAD mice, show AD symptoms later than their littermate counterparts [15]. In the end, molecular chaperone-mediated amyloidogenesis inhibition, seems to be a double-edged sword for the cell, effective, but at the same time, conditionally harmful. The inadvertent bias that pre-clinical studies introduce, using test subjects with FAD, rather than sporadic AD, could make the inhibition system seem much more flawed than it really is.

3.4. Amyloidogenesis inhibitors, derived from aggregation-prone protein regions

We ultimately proposed that the cell can prevent amyloid formation by utilizing the intrinsic amyloidogenicity of specific molecular chaperones, similar to how functional amyloids work. If that statement proves to be true, harnessing the ability of molecular chaperones to halt amyloid formation could be essential to tackling AD and other amyloidoses. The key to inhibiting amyloid formation lies in the aggregation-prone regions of said proteins, thus synthesizing and studying peptides from such regions could provide novel inhibitors of Aβ amyloidogenesis and amyloid formation in general [63].

It is worth mentioning that the ability of molecular chaperones to inhibit amyloid formation doesn't seem to be substrate-specific, meaning that one chaperone could act as an amyloidogenesis inhibitor for a variety of different amyloidogenic proteins, even if they are not known to interact *in vivo*. For example, though α-crystallin is known to interact with Aβ [50], the casein proteins are not. Despite that, all of them can inhibit Aβ amyloidogenesis *in vitro* [64,65]. Furthermore, this also seems to be the case for aggregation-prone peptides that are not derived from regions of molecular chaperones [24]. Mimicking the physiological system for amyloidogenesis prevention and extending it to aggregation-prone peptide-analogues of non-chaperone-active proteins could provide us with a much greater variety of potential inhibitors.

Despite the potential that specific peptides show as amyloidogenesis inhibitors, it is of vital importance to ensure that they are non-toxic for

the cell. It is noteworthy that, even though some molecular chaperones have amyloidogenic properties, they seem to not have negative effects on the survival of the cell. In a similar manner, functional amyloids are not harmful to the organisms in which they appear. It is believed that controlling the expression of amyloidogenic proteins, regulating fibril formation with co-localized proteins-molecules, and the fact that they are often found isolated inside membrane-bound compartments, are some of the reasons why functional amyloids are not toxic [66]. For the peptide-inhibitors to be usable, these questions must be accurately answered, and the findings should be incorporated in their implementation as potential drugs for amyloidoses, especially when it comes to peptide concentration and the complementary substances that should be administered.

4. Conclusions

Clusterin has at least five aggregation-prone regions in its α-chain and these regions may have an essential role in the inhibition of amyloid-β fibril formation. These findings hint that molecular chaperones with amyloidogenic properties might be implicated in the regulation of amyloid formation, essentially acting as functional amyloids. Harnessing the ability of molecular chaperones to halt amyloid formation could be of vital importance for the treatment of Alzheimer's disease and other amyloidoses.

5. Materials and methods

5.1. Prediction of potential aggregation-prone and clusterin AlphaFold model generation

AMYLPRED [18] was used for the identification of aggregation-prone regions in wild-type, mature clusterin (Uniprot AC: P10909 [67]). AMYLPRED makes consensus predictions of protein regions with high amyloidogenic propensity based on amino acid sequence. The threshold for making a consensus prediction is set to there being an agreement among at least 2 out of the 5 following individual methods:

- Average packing density values above threshold [68].
- Possible conformational switches detected by SecStr [69].
- Match to the amyloidogenic pattern [70].
- Tango scores above threshold [71].
- Hexapeptide conformational energy values below threshold [72].

The α-chain, which is our focus in the current study, has 5 predicted regions. The first one (^{12}NFHAMFQ^{18}) has previously been studied by our lab and proved to exhibit amyloidogenic properties *in vitro* [7]. This time, we opted to study the remaining 4, those being ^{31}MDIHF^{35}, ^{82}LSV^{84}, ^{155}YYLRVTT^{161}, and ^{177}EVVVKLF^{183}. The β-chain contains 7 more aggregation-prone regions [7], which will not be analyzed in this study.

AlphaFold-Multimer was used through ColabFold, to generate clusterin's structural model [35–39]. The α- and β-chains were individually input as different sequences to simulate the post-translational proteolytic cleavage. The signal peptide was excluded from the prediction. STRIDE [40] was used to extract secondary structure data from the AlphaFold model. Post-translational modification data were extracted through Uniprot (AC: P10909).

5.2. Peptide synthesis

All peptide-analogues were synthesized and lyophilized by GeneCust Europe, France. The exact sequences for the peptide-analogues were NFHAMFQ, AMDIHF, ILSVD, NLSVD, YYLRVTT, and EVVVKLF. The regions that were used for the second and third peptide-analogues were ^{30}AMDIHF^{35} and ^{81}ILSVD^{85}, which are extensions of the originally predicted regions. NLSVD is a mutant counterpart of ILSVD. The purity of all the synthesized peptides was higher than 98%, with the N- and C-terminals being free.

Aβ_{42} was also synthesized and lyophilized by GeneCust Europe, France. The exact sequence is DAEFRHDSGYEVHHQKLVFFAEDVGSNKGAIIGLMVGGVVIA. The purity of the peptide was higher than 95%, with the N- and C-terminals being free.

5.3. Sample preparation

5.3.1. Disaggregation of pre-existing aggregates

Each lyophilized peptide was dissolved in 1,1,1,3,3,3-Hexafluoro-2-propanol (HFIP; Sigma-Aldrich) at a concentration of 1 mg/mL. All clusterin peptides were mixed with equimolar amounts of Aβ_{42}. Individual peptide solutions and Aβ_{42}-clusterin peptide solutions were left to dry overnight in a fume hood, at room temperature, until thin peptide-containing films were created. The peptide-containing films were stored at −20 °C.

5.3.2. In vitro fibril formation

The peptide-containing films were left at room temperature for 30 min and dissolved in 0.1 M HEPES buffer (pH = 7.4; Biosera) or dH_2O (pH = 5.57), at concentrations ranging from 10 μM to 1 mM. The peptide solutions were incubated for 1 week at 37 °C unless stated otherwise.

5.4. Transmission Electron Microscopy (TEM)

A 3 μL droplet of 100 or 500 μM peptide solution was applied to glow-discharged 400-mesh carbon-coated copper grids for 60 s. Directly afterwards, the grids were stained with a 3 μL droplet of 2% (*w/v*) aqueous uranyl acetate for another 60 s. Excess stain was blotted away with filter paper and air-dried. The grids were examined with a Morgagni 268 transmission electron microscope, operated at 80 kV. Digital acquisitions were performed with an 11 Mpixel side-mounted Morada CCD camera (Soft Imaging System, Muenster, Germany).

5.5. X-ray diffraction from oriented protein fibers

5.5.1. Oriented fiber formation

1 mM peptide solutions were incubated for two weeks, to form viscous solutions, which facilitate the formation of oriented fibers. A 10 μL droplet of each peptide solution was placed between two quartz capillaries covered with wax, spaced approximately 1.5 mm apart, and mounted horizontally on a glass substrate, as collinearly as possible. The droplet was allowed to dry for 3 days until oriented fibers were formed.

5.5.2. X-ray diffraction and analysis

The oriented fibers were shot with X-rays and diffracted. The X-ray diffraction pattern was collected using a SuperNova-Agilent Technologies X-ray generator, equipped with a 135 mm ATLAS CCD detector and a 4-circle kappa goniometer, at the Institute of Biology, Medicinal Chemistry and Biotechnology, National Hellenic Research Foundation (CuKα high intensity X-ray micro-focus source, $\lambda = 1.5418$ Å), operated at 50 kV, 0.8 mA. The specimen-to-film distance was set at 52 mm and the exposure time was set to 200 s. The X-ray patterns were initially viewed using CrysAlisPro [73] and afterwards measured with iMosFLM [74].

5.6. Attenuated total reflectance Fourier-transform infrared (ATR FT-IR) spectroscopy

A 10 μL droplet of 500 μM peptide solution was cast on a front-coated Au mirror and left to dry slowly at room temperature until a thin peptide-containing film was created. Infrared spectra were obtained from these films at a resolution of 4 cm^{-1}, utilizing an IR microscope (IRScope II by Bruker Optics) equipped with a Ge attenuated total reflectance (ATR) objective lens (20×) and attached to a Fourier-

transform infrared (FT-IR) spectrometer (Equinox 55, by Bruker Optics). Ten 32-scan spectra were collected from each sample and averaged to improve the sound/noise (S/N) ratio. Both are shown in the absorption mode after correction for the wavelength dependence of the penetration depth (pd-λ). Absorption band maxima were determined from the minima in the second derivative of the corresponding spectra. Derivatives were computed analytically using routines of the Bruker OPUS/OS2 software, including smoothing over a $\pm$ 13 cm^{-1} range around each data point, performed by the Savitzky–Golay [75] algorithm. Data were visualized using OriginPro 7 (OriginLab Corporation).

5.7. Congo Red birefringence assay

A 3 μL droplet of the 500 μM peptide solution was applied to glass slides and stained with a 10 mM Congo Red (Sigma-Aldrich) solution in PBS (137 mM NaCl, 27 mM KCl, 100 mM Na_2HPO_4, 18 mM KH_2PO_4, pH = 7.4) or dH_2O for approximately 30 min. Then, they were washed several times with 90% ethanol and were left to dry approximately for 10 min. The samples were observed under bright field illumination and between crossed polars, using a Leica MZ7.5 polarizing stereomicroscope, equipped with a Sony α6000 camera.

5.8. Thioflavin T (ThT) kinetic assay

ThT fluorescence measurements were conducted at 37 °C, in black 96-well plates with flat, clear bottoms, using a Tecan Spark microplate reader. The top of the plates was sealed with microplate covers and the fluorescence readings were performed through the bottom. A 444 nm filter was used for excitation and a 484 nm filter for emission. HFIP peptide films were dissolved in DMSO (Applichem GmbH) and diluted in HEPES for a final DMSO concentration of less than 5% *v*/v. The reaction solutions contained freshly prepared 10 μM disaggregated peptide solutions (individual Aβ_{42} or Aβ_{42}-clusterin peptide solutions) and 25 μM ThT (Sigma-Aldrich) in dH_2O. ThT background fluorescence was measured in the absence of peptide solutions. Each experiment was conducted in triplicates. Measurement lasted for 50 h and fluorescence readings were collected every 15 min. ThT background fluorescence was subtracted from the peptide fluorescence readings at each time point. Standard deviation was calculated, and the data was normalized. 100 arbitrary units correspond to maximum individual Aβ_{42} fluorescence intensity. Data were visualized using RStudio (package ggplot2).

5.9. Molecular dynamics simulations

5.9.1. Structure acquisition and molecular docking

Simulations were performed using an NMR structure of pentameric Aβ_{42} (PDB ID: 2BEG) [26], while a structure for EVVVKLF was generated through the "Builder" tool in PyMOL [27]. Aβ_{42}-EVVVKLF docking was performed through the automated protein docking server ClusPro [28–31]. The generated clusters were evaluated with the balanced scoring scheme.

5.9.2. Molecular dynamics simulations

The derived complex was subjected to molecular dynamics simulations *via* GROMACS v. 2018.1 [76]. The simulations employed the AMBER99SB-ILDN protein, nucleic AMBER94 force-field [77]. The complex was placed in a 1.2 nm cubic box of 3-point model (TIP3P) water [78] and the system was ionized using NaCl molecules, mimicking neutral pH conditions. Each simulation system was subjected to energy minimization, in a maximum of 2000 steps, using the steepest descent algorithm, followed by two stages of equilibration simulations with position restraints applied on protein coordinates. Specifically, a 100 ps simulation was performed in the canonical (NVT) ensemble to equilibrate temperature at 310 K, using the Berendsen-thermostat [79]. Following the first equilibration, a 100 ps simulation was performed in the isothermal-isobaric (NPT) ensemble to control pressure isotopically at 1.013 bar (1 atm), using the Berendsen weak coupling algorithm [80] and the Berendsen-thermostat at 310 K. Finally, the MD simulation with position restraints removed was carried out for 600 ns at 310 K. One control run of individual Aβ_{42} was also performed. Periodic boundary conditions were applied to all directions. The LINCS algorithm [81] was applied to model bond constraints, enabling the use of a 2 fs time-step. Short-range non-bonded interactions were modeled using a twin-range cutoff at 0.8 nm, while long-range electrostatic interactions were modeled using the Particle Mesh Ewald (PME) method, with a Fourier grid spacing at 0.12 nm [82].

5.9.3. Analysis of simulation results

Simulation results were analyzed using various GROMACS utilities, and Visual Molecular Dynamics (VMD) v. 1.9.4 [83]. Structural stability was checked using the "rms" tool [84]. Secondary structure was calculated using the "do_dssp" tool [32,33]. Hydrogen bonds were calculated using the "hbond" tool [85]. Frames were extracted every 100 ps and used for the analysis. Pictures were collected with UCSF Chimera [34] or PyMOL [27].

CRediT authorship contribution statement

Panagiotis M. Spatharas: Conceptualization, Methodology, Validation, Investigation, Writing – original draft. **Georgia I. Nasi:** Methodology, Validation, Investigation, Writing – review & editing. **Paraskevi L. Tsiolaki:** Conceptualization, Validation, Methodology, Writing – review & editing. **Marilena K. Theodoropoulou:** Investigation, Writing – review & editing. **Nikos C. Papandreou:** Validation, Writing – review & editing. **Andreas Hoenger:** Validation, Writing – review & editing. **Ioannis P. Trougakos:** Conceptualization, Resources, Writing – review & editing. **Vassiliki A. Iconomidou:** Conceptualization, Methodology, Validation, Resources, Supervision, Writing – review & editing, Funding acquisition.

Declaration of competing interest

The authors declare the following financial interests/personal relationships which may be considered as potential competing interests: Vassiliki Iconomidou reports financial support was provided by European Union and Greek national funds.

Acknowledgments

This research has been co-financed by the European Union and Greek national funds through the Operational Program "Competitiveness, Entrepreneurship and Innovation", under the call "RESEARCH – CREATE – INNOVATE" (project code: T1EDK-00353). We acknowledge support of this work by the project "INSPIRED-The National Research Infrastructures on Integrated Structural Biology, Drug Screening Efforts and Drug target functional characterization" (MIS 5002550) which is implemented under the Action "Reinforcement of the Research and Innovation Infrastructure", funded by the Operational Program "Competitiveness, Entrepreneurship and Innovation" (NSRF 2014-2020) and co-funded by Greece and the European Union (European Regional Development Fund). The molecular dynamics simulations were performed utilizing computational time granted from the Greek Research & Technology Network (GRNET) at the National HPC facility – ARIS under project ID "PR007003-AbetaDynamics". We also acknowledge Dr. George Baltatzis for kindly assisting us with handling the Morgagni Microscope at the 1st Department of Pathology, Medical School, National and Kapodistrian University of Athens. Finally, we acknowledge the support of Dr. Aimilia Sklirou, who kindly assisted with handling the Tecan Spark microplate reader.

Appendix A. Supplementary data

Supplementary data to this article can be found online at https://doi.org/10.1016/j.bbadis.2022.166384.

References

[1] R.A. Kyle, Amyloidosis: a brief history, Amyloid 18 (Suppl 1) (2011) 6–7.
[2] M.D. Benson, J.N. Buxbaum, D.S. Eisenberg, G. Merlini, M.J.M. Saraiva, Y. Sekijima, et al., Amyloid nomenclature 2020: update and recommendations by the International Society of Amyloidosis (ISA) nomenclature committee, Amyloid 27 (2020) 217–222.
[3] A. Wentink, C. Nussbaum-Krammer, B. Bukau, Modulation of amyloid states by molecular chaperones, Cold Spring Harb. Perspect. Biol. 11 (7) (2019) a033969.
[4] T.A. Niewold, C.L. Murphy, C.A. Hulskamp-Koch, P.C. Tooten, E. Gruys, Casein related amyloid, characterization of a new and unique amyloid protein isolated from bovine corpora amylacea, Amyloid 6 (1999) 244–249.
[5] H. Ecroyd, J.A. Carver, Crystallin proteins and amyloid fibrils, Cell. Mol. Life Sci. 66 (2009) 62–81.
[6] H. Ecroyd, D.C. Thorn, Y. Liu, J.A. Carver, The dissociated form of kappa-casein is the precursor to its amyloid fibril formation, Biochem. J. 429 (2010) 251–260.
[7] P.L. Tsiolaki, K.C. Nastou, N.N. Louros, S.J. Hamodrakas, V.A. Iconomidou, Exploring amyloidogenicity of clusterin: a structural and bioinformatics analysis, Adv. Exp. Med. Biol. 989 (2017) 93–107.
[8] S.E. Jones, C. Jomary, Clusterin, Int. J. Biochem. Cell Biol. 34 (2002) 427–431.
[9] R.W. Bailey, A.K. Dunker, C.J. Brown, E.C. Garner, M.D. Griswold, Clusterin, a binding protein with a molten globule-like region, Biochemistry 40 (2001) 11828–11840.
[10] S. Poon, M.S. Rybchyn, S.B. Easterbrook-Smith, J.A. Carver, G.J. Pankhurst, M. R. Wilson, Mildly acidic pH activates the extracellular molecular chaperone clusterin, J. Biol. Chem. 277 (2002) 39532–39540.
[11] S. Poon, S.B. Easterbrook-Smith, M.S. Rybchyn, J.A. Carver, M.R. Wilson, Clusterin is an ATP-independent chaperone with very broad substrate specificity that stabilizes stressed proteins in a folding-competent state, Biochemistry 39 (2000) 15953–15960.
[12] M. Calero, A. Rostagno, B. Frangione, J. Ghiso, Clusterin and Alzheimer's disease, Subcell. Biochem. 38 (2005) 273–298.
[13] P. Rohne, H. Prochnow, C. Koch-Brandt, The CLU-files: disentanglement of a mystery, Biomol. Concepts 7 (2016) 1–15.
[14] E. Matsubara, C. Soto, S. Governale, B. Frangione, J. Ghiso, Apolipoprotein J and Alzheimer's amyloid beta solubility, Biochem. J. 316 (Pt 2) (1996) 671–679.
[15] S.B. Oh, M.S. Kim, S. Park, H. Son, S.Y. Kim, M.S. Kim, et al., Clusterin contributes to early stage of Alzheimer's disease pathogenesis, Brain Pathol. 29 (2019) 217–231.
[16] R.B. DeMattos, M.A. O'Dell, M. Parsadanian, J.W. Taylor, J.A. Harmony, K.R. Bales, et al., Clusterin promotes amyloid plaque formation and is critical for neuritic toxicity in a mouse model of Alzheimer's disease, Proc. Natl. Acad. Sci. U. S. A. 99 (2002) 10843–10848.
[17] K.C. Nastou, G.I. Nasi, P.L. Tsiolaki, Z.I. Litou, V.A. Iconomidou, AmyCo: the amyloidoses collection, Amyloid 26 (2019) 112–117.
[18] K.K. Frousios, V.A. Iconomidou, C.M. Karletidi, S.J. Hamodrakas, Amyloidogenic determinants are usually not buried, BMC Struct. Biol. 9 (2009) 44.
[19] M. Sunde, C.C. Blake, From the globular to the fibrous state: protein structure and structural conversion in amyloid formation, Q. Rev. Biophys. 31 (1998) 1–39.
[20] O.S. Makin, L.C. Serpell, X-ray diffraction studies of amyloid structure, Methods Mol. Biol. 299 (2005) 67–80.
[21] W.K. Surewicz, H.H. Mantsch, D. Chapman, Determination of protein secondary structure by Fourier transform infrared spectroscopy: a critical assessment, Biochemistry 32 (1993) 389–394.
[22] K. Bettens, S. Vermeulen, C. Van Cauwenberghe, B. Heeman, B. Asselbergh, C. Robberecht, et al., Reduced secreted clusterin as a mechanism for Alzheimer-associated CLU mutations, Mol. Neurodegener. 10 (2015) 30.
[23] J.J. Yerbury, S. Poon, S. Meehan, B. Thompson, J.R. Kumita, C.M. Dobson, et al., The extracellular chaperone clusterin influences amyloid formation and toxicity by interacting with prefibrillar structures, FASEB J. 21 (2007) 2312–2322.
[24] J. Lu, Q. Cao, C. Wang, J. Zheng, F. Luo, J. Xie, et al., Structure-based peptide inhibitor design of amyloid-beta aggregation, Front. Mol. Neurosci. 12 (2019) 54.
[25] S.M. Chafekar, H. Malda, M. Merkx, E.W. Meijer, D. Viertl, H.A. Lashuel, et al., Branched KLVFF tetramers strongly potentiate inhibition of beta-amyloid aggregation, ChemBioChem 8 (2007) 1857–1864.
[26] T. Luhrs, C. Ritter, M. Adrian, D. Riek-Loher, B. Bohrmann, H. Dobeli, et al., 3D structure of Alzheimer's amyloid-beta(1–42) fibrils, Proc. Natl. Acad. Sci. U. S. A. 102 (2005) 17342–17347.
[27] W.L. Delano, The PyMOL Molecular Graphics System, DeLano Scientific LLC, 400, Oyster Point Blvd., Suite 213, South San Francisco, CA 94080-1918, USA, 2005.
[28] D. Kozakov, D. Beglov, T. Bohnuud, S.E. Mottarella, B. Xia, D.R. Hall, et al., How good is automated protein docking? Proteins 81 (2013) 2159–2166.
[29] D. Kozakov, D.R. Hall, B. Xia, K.A. Porter, D. Padhorny, C. Yueh, et al., The ClusPro web server for protein-protein docking, Nat. Protoc. 12 (2017) 255–278.
[30] K.A. Porter, B. Xia, D. Beglov, T. Bohnuud, N. Alam, O. Schueler-Furman, et al., ClusPro PeptiDock: efficient global docking of peptide recognition motifs using FFT, Bioinformatics 33 (2017) 3299–3301.
[31] S. Vajda, C. Yueh, D. Beglov, T. Bohnuud, S.E. Mottarella, B. Xia, et al., New additions to the ClusPro server motivated by CAPRI, Proteins 85 (2017) 435–444.
[32] W. Kabsch, C. Sander, Dictionary of protein secondary structure: pattern recognition of hydrogen-bonded and geometrical features, Biopolymers 22 (1983) 2577–2637.
[33] W.G. Touw, C. Baakman, J. Black, T.A.H. te Beek, E. Krieger, R.P. Joosten, et al., A series of PDB-related databanks for everyday needs, Nucleic Acids Res. 43 (2015) D364–D368.
[34] E.F. Pettersen, T.D. Goddard, C.C. Huang, G.S. Couch, D.M. Greenblatt, E.C. Meng, et al., UCSF Chimera?A visualization system for exploratory research and analysis, J. Comput. Chem. 25 (2004) 1605–1612.
[35] M Mirdita K Schütze Y Moriwaki L Heo S Ovchinnikov M. Steinegger ColabFold - Making protein folding accessible to all. bioRxiv. 2021:2021.08.15.456425.
[36] R Evans M O'Neill A Pritzel N Antropova A Senior T Green et alProtein complex prediction with AlphaFold-Multimer. bioRxiv. 2021:2021.10.04.463034.
[37] A.L. Mitchell, A. Almeida, M. Beracochea, M. Boland, J. Burgin, G. Cochrane, et al., MGnify: the microbiome analysis resource in 2020, Nucleic Acids Res. 48 (2020) D570–D578.
[38] M. Mirdita, M. Steinegger, J. Soding, MMseqs2 desktop and local web server app for fast, interactive sequence searches, Bioinformatics 35 (2019) 2856–2858.
[39] M. Mirdita, L. von den Driesch, C. Galiez, M.J. Martin, J. Soding, M. Steinegger, Uniclust databases of clustered and deeply annotated protein sequences and alignments, Nucleic Acids Res. 45 (2017) D170–D176.
[40] M. Heinig, D. Frishman, STRIDE: a web server for secondary structure assignment from known atomic coordinates of proteins, Nucleic Acids Res. 32 (2004) W500–W502.
[41] P.K. Teng, D. Eisenberg, Short protein segments can drive a non-fibrillizing protein into the amyloid state, Protein Eng. Des. Sel. 22 (2009) 531–536.
[42] X.M. Qi, C. Wang, X.K. Chu, G. Li, J.F. Ma, Intraventricular infusion of clusterin ameliorated cognition and pathology in Tg6799 model of Alzheimer's disease, BMC Neurosci. 19 (2018) 2.
[43] J.J. Yerbury, J.R. Kumita, Protein chemistry of amyloid fibrils and chaperones: implications for amyloid formation and disease, Curr. Chem. Biol. 4 (2010) 89–98.
[44] S. Meehan, Y. Berry, B. Luisi, C.M. Dobson, J.A. Carver, C.E. MacPhee, Amyloid fibril formation by lens crystallin proteins and its implications for cataract formation, J. Biol. Chem. 279 (2004) 3413–3419.
[45] E. Basha, H. O'Neill, E. Vierling, Small heat shock proteins and alpha-crystallins: dynamic proteins with flexible functions, Trends Biochem. Sci. 37 (2012) 106–117.
[46] J.A. Carver, A. Rekas, D.C. Thorn, M.R. Wilson, Small heat-shock proteins and clusterin: intra- and extracellular molecular chaperones with a common mechanism of action and function? IUBMB Life 55 (2003) 661–668.
[47] M. Haslbeck, J. Buchner, Chaperone function of sHsps, Prog. Mol. Subcell. Biol. 28 (2002) 37–59.
[48] R. Inoue, T. Takata, N. Fujii, K. Ishii, S. Uchiyama, N. Sato, et al., New insight into the dynamical system of alphaB-crystallin oligomers, Sci. Rep. 6 (2016) 29208.
[49] E.W. Doss, K.A. Ward, J.F. Koretz, Preliminary studies on the aggregation process of alpha-crystallin, Exp. Eye Res. 65 (1997) 255–266.
[50] P. Narayan, S. Meehan, J.A. Carver, M.R. Wilson, C.M. Dobson, D. Klenerman, Amyloid-beta oligomers are sequestered by both intracellular and extracellular chaperones, Biochemistry 51 (2012) 9270–9276.
[51] M. Cheon, I. Chang, S. Mohanty, L.M. Luheshi, C.M. Dobson, M. Vendruscolo, et al., Structural reorganisation and potential toxicity of oligomeric species formed during the assembly of amyloid fibrils, PLoS Comput. Biol. 3 (2007) 1727–1738.
[52] C. Kunz, B. Lonnerdal, Human-milk proteins: analysis of casein and casein subunits by anion-exchange chromatography, gel electrophoresis, and specific staining methods, Am. J. Clin. Nutr. 51 (1990) 37–46.
[53] D.J. McMahon, B.S. Oommen, Supramolecular structure of the casein micelle, J. Dairy Sci. 91 (2008) 1709–1721.
[54] E.M. Redwan, B. Xue, H.A. Almehdar, V.N. Uversky, Disorder in milk proteins: caseins, intrinsically disordered colloids, Curr. Protein Pept. Sci. 16 (2015) 228–242.
[55] P.E. Morgan, T.M. Treweek, R.A. Lindner, W.E. Price, J.A. Carver, Casein proteins as molecular chaperones, J. Agric. Food Chem. 53 (2005) 2670–2683.
[56] D.C. Thorn, H. Ecroyd, M. Sunde, S. Poon, J.A. Carver, Amyloid fibril formation by bovine milk alpha s2-casein occurs under physiological conditions yet is prevented by its natural counterpart, alpha s1-casein, Biochemistry 47 (2008) 3926–3936.
[57] D.C. Thorn, S. Meehan, M. Sunde, A. Rekas, S.L. Gras, C.E. MacPhee, et al., Amyloid fibril formation by bovine milk kappa-casein and its inhibition by the molecular chaperones alphaS- and beta-casein, Biochemistry 44 (2005) 17027–17036.
[58] Y. Su, P.T. Chang, Acidic pH promotes the formation of toxic fibrils from beta-amyloid peptide, Brain Res. 893 (2001) 287–291.
[59] M. Beeg, M. Stravalaci, M. Romeo, A.D. Carra, A. Cagnotto, A. Rossi, et al., Clusterin binds to Abeta1-42 oligomers with high affinity and interferes with peptide aggregation by inhibiting primary and secondary nucleation, J. Biol. Chem. 291 (2016) 6958–6966.
[60] S.F. de Retana, P. Marazuela, M. Sole, G. Colell, A. Bonaterra, J.L. Sanchez-Quesada, et al., Peripheral administration of human recombinant ApoJ/clusterin modulates brain beta-amyloid levels in APP23 mice, Alzheimers Res. Ther. 11 (2019) 42.
[61] L. Wu, P. Rosa-Neto, G.Y. Hsiung, A.D. Sadovnick, M. Masellis, S.E. Black, et al., Early-onset familial Alzheimer's disease (EOFAD), Can. J. Neurol. Sci. 39 (2012) 436–445.
[62] F.M. LaFerla, K.N. Green, Animal models of Alzheimer disease, Cold Spring Harb. Perspect. Med. 2 (2012).
[63] S. Connelly, S. Choi, S.M. Johnson, J.W. Kelly, I.A. Wilson, Structure-based design of kinetic stabilizers that ameliorate the transthyretin amyloidoses, Curr. Opin. Struct. Biol. 20 (2010) 54–62.

[64] R. Carrotta, C. Canale, A. Diaspro, A. Trapani, P.L. Biagio, D. Bulone, Inhibiting effect of alpha(s1)-casein on Abeta(1–40) fibrillogenesis, Biochim. Biophys. Acta 1820 (2012) 124–132.
[65] B. Raman, T. Ban, M. Sakai, S.Y. Pasta, T. Ramakrishna, H. Naiki, et al., AlphaB-crystallin, a small heat-shock protein, prevents the amyloid fibril growth of an amyloid beta-peptide and beta2-microglobulin, Biochem. J. 392 (2005) 573–581.
[66] M.P. Jackson, E.W. Hewitt, Why are functional amyloids non-toxic in humans? Biomolecules 7 (2017).
[67] C. UniProt, UniProt: the universal protein knowledgebase in 2021, Nucleic Acids Res. 49 (2021) D480–D489.
[68] O.V. Galzitskaya, S.O. Garbuzynskiy, M.Y. Lobanov, Prediction of amyloidogenic and disordered regions in protein chains, PLoS Comput. Biol. 2 (2006), e177.
[69] S.J. Hamodrakas, C. Liappa, V.A. Iconomidou, Consensus prediction of amyloidogenic determinants in amyloid fibril-forming proteins, Int. J. Biol. Macromol. 41 (2007) 295–300.
[70] M. Lopez de la Paz, L. Serrano, Sequence determinants of amyloid fibril formation, Proc. Natl. Acad. Sci. U. S. A. 101 (2004) 87–92.
[71] A.M. Fernandez-Escamilla, F. Rousseau, J. Schymkowitz, L. Serrano, Prediction of sequence-dependent and mutational effects on the aggregation of peptides and proteins, Nat. Biotechnol. 22 (2004) 1302–1306.
[72] Z. Zhang, H. Chen, L. Lai, Identification of amyloid fibril-forming segments based on structure and residue-based statistical potential, Bioinformatics 23 (2007) 2218–2225.
[73] CrysAlisPRO, Agilent Technologies. Version 1.171.37.31, ed, Agilent Technologies UK Ltd, Oxford, UK, 2014. p. Software system.
[74] T.G. Battye, L. Kontogiannis, O. Johnson, H.R. Powell, A.G. Leslie, iMOSFLM: a new graphical interface for diffraction-image processing with MOSFLM, Acta Crystallogr. D Biol. Crystallogr. 67 (2011) 271–281.
[75] A. Savitzky, M.J.E. Golay, Smoothing and differentiation of data by simplified least squares procedures, Anal. Chem. 36 (1964) 1627–1639.
[76] C. Kutzner, S. Pall, M. Fechner, A. Esztermann, B.L. de Groot, H. Grubmuller, More bang for your buck: improved use of GPU nodes for GROMACS 2018, J. Comput. Chem. 40 (2019) 2418–2431.
[77] K. Lindorff-Larsen, S. Piana, K. Palmo, P. Maragakis, J.L. Klepeis, R.O. Dror, et al., Improved side-chain torsion potentials for the Amber ff99SB protein force field, Proteins 78 (2010) 1950–1958.
[78] W.L. Jorgensen, J. Chandrasekhar, J.D. Madura, R.W. Impey, M.L. Klein, Comparison of simple potential functions for simulating liquid water, J. Chem. Phys. 79 (1983).
[79] H.J.C. Berendsen, J.P.M. Postma, W.F. Van Gunsteren, A. Dinola, J.R. Haak, Molecular dynamics with coupling to an external bath, J. Chem. Phys. 81 (1984).
[80] H.J.C. Berendsen, Transport properties computed by linear response through weak coupling to a bath, in: Computer Simulation in Materials Science, Springer, Dordrecht, 1991, pp. 139–155.
[81] H.B. Berk Hess, Herman J.C. Berendsen, Johannes G.E.M. Fraaije, LINCS: a linear constraint solver for molecular simulations, J. Comput. Chem. 18 (1997) 1463–1472.
[82] U. Essmann, L. Perera, M.L. Berkowitz, T. Darden, H. Lee, L.G. Pedersen, A smooth particle mesh Ewald method, J. Chem. Phys. 103 (1995).
[83] W. Humphrey, A. Dalke, K. Schulten, VMD: visual molecular dynamics, J. Mol. Graph. 14 (33–8) (1996) 27–28.
[84] V.N. Maiorov, G.M. Crippen, Size-independent comparison of protein three-dimensional structures, Proteins Struct. Funct. Genet. 22 (1995) 273–283.
[85] D. van der Spoel, P.J. van Maaren, P. Larsson, N. Tîmneanu, Thermodynamics of hydrogen bonding in hydrophilic and hydrophobic media, J. Phys. Chem. B 110 (2006) 4393–4398.